JOURNAL OF GEOPHYSICAL RESEARCH, VOL. 97, NO. B1, PAGES 569–585, JANUARY 10, 1992

Rift Flank Uplifts and Hinterland Basins: Comparison of the Transantarctic Mountains With the Great Escarpment of Southern Africa

URI TEN BRINK[1]

Department of Geophysics, Stanford University, Stanford, California

TIM STERN

Geology and Geophysics Division, Department of Scientific and Industrial Research, Wellington, New Zealand

Uplifted rift margins are a common feature of continents and oceans. Two variants of rift flank morphologies have been recognized: One in which the topography warps down from an inland high toward the continental margin, and one where the tropographic peak lies close to the continental margin. The Great Escarpment of southern Africa and the Transantarctic Mountains are examples of the first and the second variants of rift flanks, respectively. Both rift flanks are bordered on their landward side by broad continental basins: the Kalahari and the Wilkes hinterland basins. If these basins are interpreted as flexural "outer lows" that deepen in unison with the uplift of the rift flanks, the lithosphere on the uplifted side is very rigid in both cases (elastic thickness T_e of 100 ± 20 km for southern Africa and 110 ± 20 km for East Antarctica). We suggest that the variation in rift flank morphology is caused by the isostatic response to uplift forces of elastic plates sharing different boundary conditions. We model the uplift of the Transantarctic Mountains as an upward deflection of an elastic plate which is broken at the front of the Transantarctic Mountains, and we model the uplift of the Great Escarpment as an upward deflection of a continuous elastic plate that is modified by the downward load of sediments on the continental margin. Although the Transantarctic Mountain uplift is young (60–0 Ma) and the southern African uplift is old (<100 Ma), the different isostatic responses of the two margins are not a function of age, because most loading (sedimentation) and unloading (erosion) took place shortly after rifting. Detailed modeling of topography, gravity, geological markers, and the locations of depocenters suggests that lithospheric rigidity decreases under the Transantarctic Mountains, whereas in southern Africa the decrease occurs not under the Great Escarpment but far seaward under the continental shelf and slope. If the distribution of lithospheric rigidity is indicative of the thermal regime of the lithosphere, then uplifted rift flanks are not always underlain by a thermal anomaly. This and other geological evidence indicate that a single mechanism cannot explain the uplift of both the Antarctic and the African margins.

INTRODUCTION

The building of many mountain belts, such as the Andes and the Himalayas, is commonly associated with plate convergence. Another class of mountain belts, rift flank uplifts, evolves, however, at sites where plates diverge. Whereas cordilleran and collision-type mountains are the result of horizontal compression, the cause for rift flank uplifts is hotly debated. Uplift may be caused by one or more of the following forces: forces of thermal origin [*Smith and Drewry*, 1984; *Steckler*, 1985; *Buck*, 1986], mechanical or isostatic forces [*Heiskanen and Vening-Meinesz*, 1958; *Zuber and Parmentier*, 1986; *Braun and Beaumont*, 1989; *Weissel and Karner*, 1989], magmatic thickening of the crust under rift flanks ("underplating") [e.g., *Cox*, 1980], and erosion [*King*, 1955; *Ollier*, 1985; *Brown*, 1991]. Uplift forces often cannot be directly related to surface observations, such as morphology, gravity field, stratigraphy of sedimentary basins, faulting, and folding, because the isostatic response of the lithosphere acts as a filter between the uplift forces and their observed products. In studying rift flank uplifts, it is therefore necessary to first quantify the isostatic response of the underlying lithosphere.

Geomorphologists have recognized two types of rift flank morphologies. One, exemplified by the Great Escarpment of southern Africa and by the uplift of eastern Australia, is characterized by warping down of the topography toward the margin [*Ollier*, 1985]. The other, which is typical of the Transantarctic Mountains, the Western Ghats of India, and the Serra do Mar of Brazil, is characterized by a rising flank toward the continental edge [*Ollier*, 1985]. This paper compares two of the largest rift shoulder uplifts in the world which have contrasting morphologies and geological histories, the Transantarctic Mountains and the Great Escarpment of southern Africa (Figure 1). It explains the two variants of rift morphologies by the different isostatic responses of their respective lithosphere to uplift forces. The morphology of southern Africa is modeled by a continuous elastic plate across the continental margin, whereas the morphology of the Transantarctic Mountains is modeled by an elastic plate broken at the eastern edge of the mountains.

King [1955] suggested that the morphology of southern Africa is due to flexure of an elastic lithosphere which was subjected to erosion along its rifted periphery. *Stern and ten Brink* [1989] modeled the uplift of the Transantarctic Mountains as a broken elastic plate. The following study examines and quantifies King's suggestion and substantiates Stern and

[1]Now at U.S. Geological Survey, Woods Hole, Massachusetts.

Paper number 91JB02231.
0148-0227/92/91JB-02231$05.00

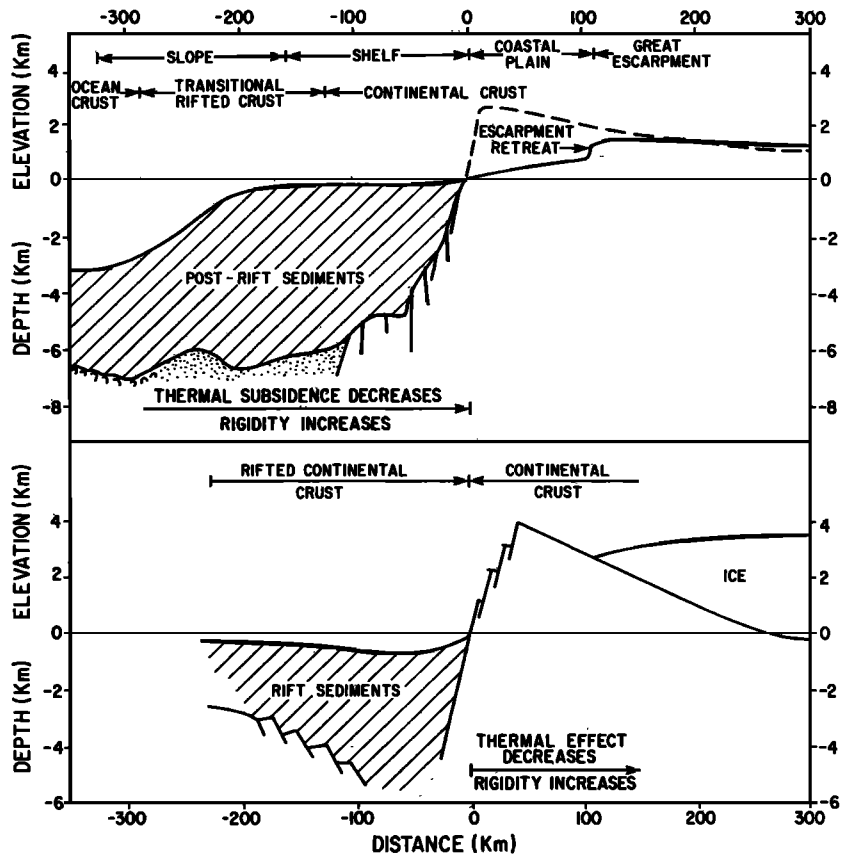

Fig. 1. Diagrammatic cross sections of the Great Escarpment of southern Africa and adjacent continental margin (top) and the Transantarctic Mountains and adjacent Ross Embayment (bottom). These cross sections represent two different types of rift flank morphologies [*Ollier*, 1985]. Dashed line is assumed initial rift flank uplift before modification by erosion and deposition. Offshore sections are based on *Austin and Uchupi* [1982] and *Gerrard and Smith* [1983] for the Atlantic coast of southern Africa and *Cooper et al.* [1987] for the Ross Sea. Onshore sections are based on models in this study.

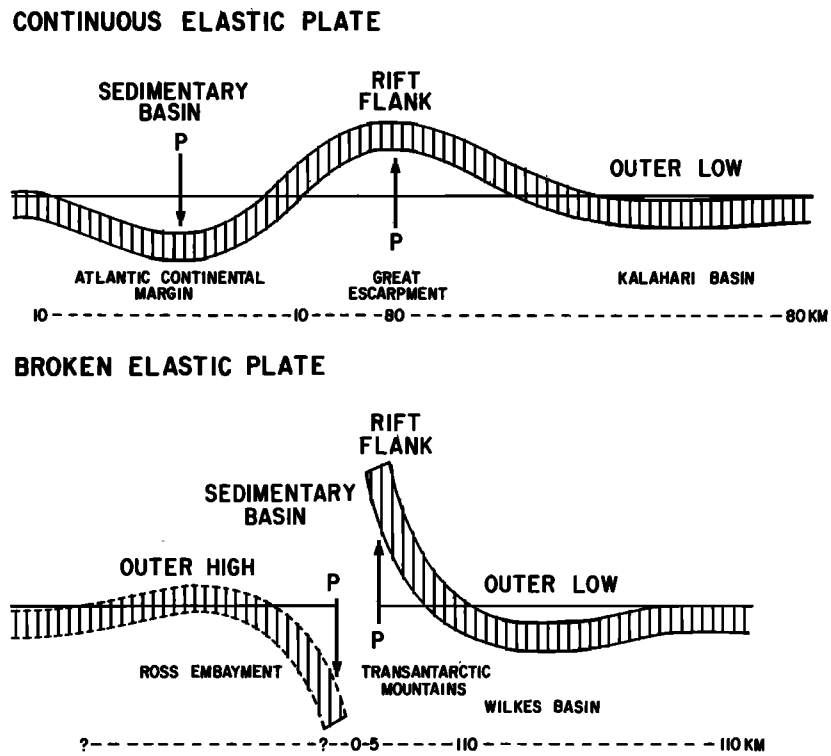

Fig. 2. Illustrations of continuous and broken elastic plate models that are subjected to upward and downward loads (P). Elastic thicknesses used for modeling the southern Africa and Antarctic uplifts are shown below the illustrations.

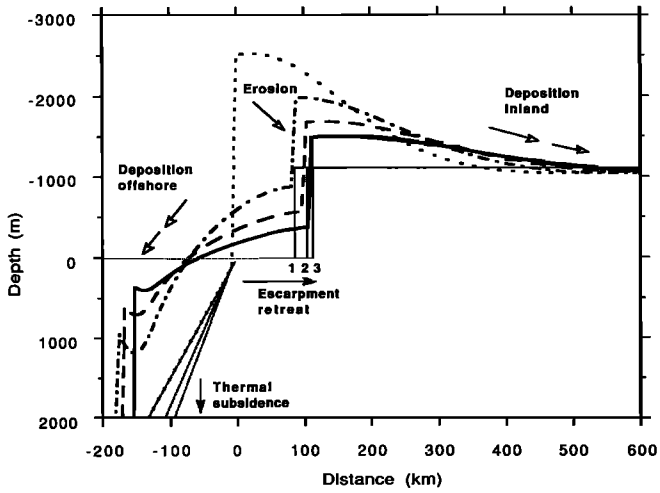

Fig. 3. Evolution of the continuous plate model through time. The initial uplift profile (heavy dotted line) is eroded by three erosional cycles, and the topography is allowed to rebound by regional isostasy after each cycle (other heavy lines). During the first cycle, the initial uplift is eroded down to the light dotted line (sea level seaward of point 1, 1000 m high landward of point 1), and the topography rebounds back to heavy dash-dotted line. Similarly, during the second cycle, the dash-dotted line is eroded to sea level seaward of the point 2, mimicking the retreat of the Great Escarpment, and to 1000 m high landward of point 2, and the topography rebounds back to heavy dashed line, and so on. Heavy continuous line is final topography. The eroded material fills inland topography below 1000 m, and the remaining material builds the continental shelf. The continental margin subsides thermally as shown as well as being depressed by sediments.

ten Brink's results. We start by presenting a conceptual model to illustrate the major difference between the two rift flank uplifts. We then review the pertinent geological evidence for the two contrasting forms of continental margins and model the detailed variations in flexural rigidity from continent to ocean using available geological constraints. Modeling of hinterland basins is incorporated into the study because we view the entire ~1200-km-wide zone, which includes the hinterland basin, the rift flank uplift, and the continental margin, as one system that is interconnected by regional lithospheric response and by erosion and sedimentation. The discussion addresses the forces causing rift flank uplifts, in particular, those of Antarctica and southern Africa, and the significance of hinterland basins. The appendices elaborate on the role of erosion in uplift and on the possible uplift forces for the Transantarctic Mountains.

Conceptual Model

We can model the two variants of rift flank morphologies as a continuous elastic plate across the continental margin of southern Africa and as a broken elastic plate across the boundary between East and West Antarctica (Figure 2). Modeling is carried out with a finite difference routine (modified from *Bodine et al.* [1981]) to calculate the deflection of the elastic plate. The finite difference routine allows for lateral variations in flexural rigidity, load distribution, and restoring force. For the continuous plate, the two ends of the plate are far from the rift flank uplift (approximately eight wavelengths) and the deflection y and its second derivative at the two ends equal zero. For the broken plate, one end of the plate is far from the rift flank uplift and has the above boundary conditions, but at the end located at the boundary between East and West Antarctica, the total moments and shear stresses equal zero (i.e., $y'' = y''' = 0$).

Modeling the Transantarctic Mountains as a broken elastic plate is relatively simple. It involves the application of an uplift force that is ascribed to a combination of forces arising from erosion, isostatic forces, and thermal conduction of heat from West to East Antarctica (Appendix A and *Stern and ten Brink* [1989]). In contrast, the continuous plate model for southern Africa is more problematic because erosion of the rift flank uplift and subsequent sediment loading at the continental margin act as additional forces that modify the uplift profile through time. The time development of the model for southern Africa can be described as follows (Figure 3): Following the application of an initial uplift force, the Great Escarpment retreats from the coast inland in three steps in which erosion bevels the topography to sea level seaward of the escarpment and to an elevation of 1000 m landward of the escarpment. The topography is allowed to rebound by regional isostasy after each step. Uplift of the escarpment induces a flexural downwarp in the hinterland, which is filled by the eroded material to an elevation of 1000 m. The remainder (majority) of the eroded material fills the continental margin, and the topography is adjusted isostatically for sediment loading. Sediments fill the margin to sea level, and the margin progrades far enough seaward to accommodate all the available sediments. In conjunction with erosion and deposition at each step, the continental margin subsides tectonically as a result of time-dependent lithospheric cooling. Geological constraints and further details of the modeling parameters are described later in the text.

Two "time-dependent" end-member models are compared in Figure 4. In one model, the plate is continuous across the continental margin and has an elastic thickness T_e

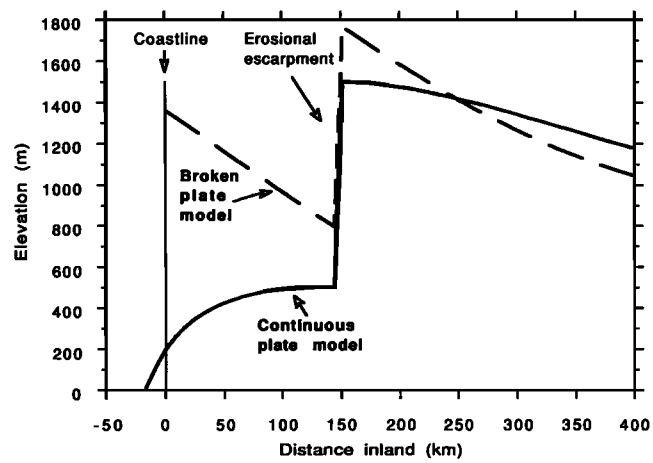

Fig. 4. Comparison between the predicted final topography of rift flank uplifts from continuous and broken elastic plate models. The topography from the continuous plate model resembles the topography of the Great Escarpment (Figure 1), whereas the topography from the broken plate model resembles the topography of the Transantarctic Mountains. The models include initial uplifts followed by three steps of escarpment erosion and deposition offshore and in the hinterland basin (Figure 3). Elastic thickness for both models is 80 km onshore decreasing to T_e = 30 km at 125 km seaward of the coast for the continuous plate model and dropping to T_e = 0 km at the coast for the broken plate model.

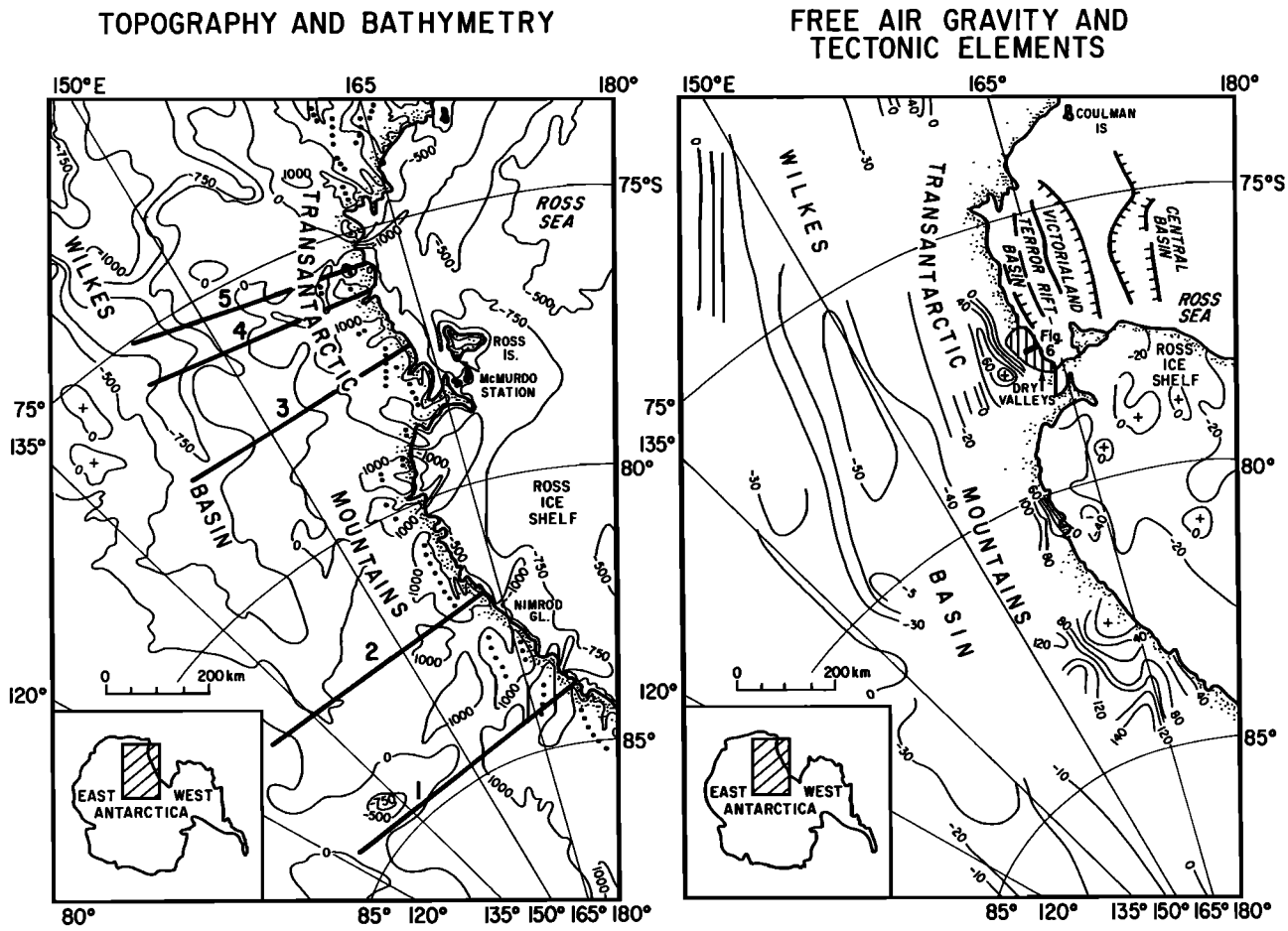

Fig. 5. (Left) Simplified bedrock topography and bathymetry of the Transantarctic Mountains, the Wilkes Basin, and the Western Ross Sea [after *Drewry*, 1983]. Heavy line is approximate coastline. Dotted lines are highest peaks of the mountains. Numbered heavy solid lines are location of the five topographic profiles that are shown stacked in Figure 7. (Right) tectonic elements of the Ross Sea [after *Cooper et al.*, 1991] and free-air gravity anomaly map over ice-covered areas (compiled from *Davey* [1981]; and *Groushinsky and Sazhina* [1978]). Shaded area is dry valleys. Heavy line in dry valleys is location of Figure 6.

of 30 km under the continental margin. In the other model, the continent is broken at the coast (i.e., T_e = 0 km at the continental margin). In the broken plate model, sediments deposited offshore do not affect the isostatic movements onshore, whereas in the continuous plate model, sediment loading offshore deflects the coastal plain. As a result, the predicted topography in the broken plate model (T_e = 0 km) rises from the Great Escarpment seaward so that the elevation at the coast is almost as high as in the Great Escarpment. In contrast, the topography of the continuous plate model (T_e = 30 km) decreases in elevation toward the coast. The decrease in elevation toward the coast in the continuous plate model is caused by the weight of the sediments on the continental margin (Figure 2). The sediments act as a downward force depressing the nearby coastal uplift and subduing rebound due to erosion. Both the present elevation and elevations of older erosional surfaces and other geological markers in southern Africa decrease toward the coast much like the predictions of the continuous plate models. In detail, the African erosional surface is convex between the Great Escarpment and the coast [*King*, 1955; *Partridge and Maud*, 1987] similar to the predicted topography profile. The broken plate model fits better the geometry of the Transantarctic Mountains front where the topography rises inland in a series of landward tilted blocks, separated by normal faults.

Regional Geology and Isostatic Models

The Transantarctic Mountains

The Transantarctic Mountains (Figure 5*a*), with a length of about 3000 km and elevations of up to 4500 m, is one of the largest of the rift flank uplift in the world. This mountain range is located on the East Antarctic craton at its boundary with West Antarctica. Thrusting and folding, which characterize orogenic mountain belts, are not observed in the Transantarctic Mountains [*Smith and Drewry*, 1984]. Rather, the building of this mountain range was accompanied by normal faulting and a gentle asymmetric tilt of strata to the west (Figure 6). The boundary between East and West Antarctica (located at the mountain front and the nearby offshore) is characterized by a narrow (<60 km) zone of extensive normal faults [*Gleadow and Fitzgerald*, 1987; *Behrendt and Cooper*, 1991] and by a steep (2–7 mGal/km) gravity gradient [*Kienle et al.*, 1989]. West Antarctica adja-

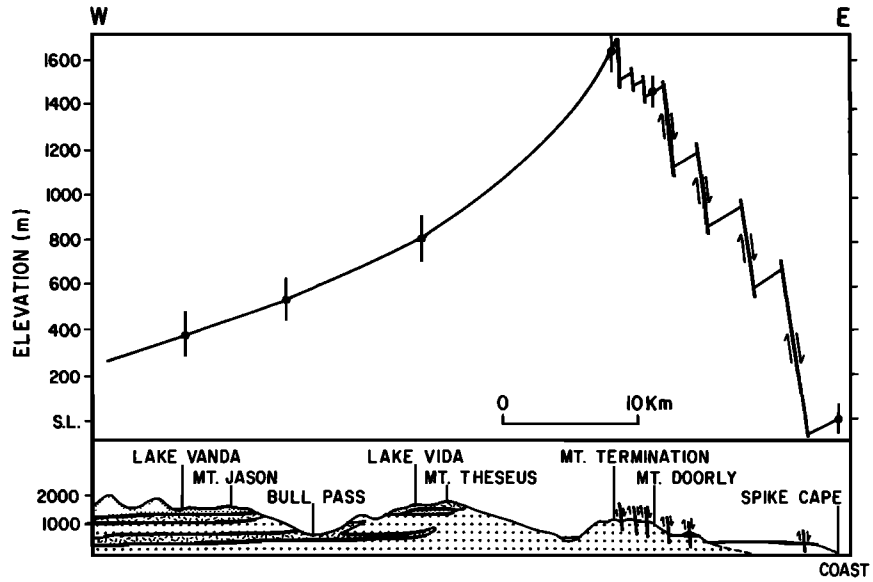

Fig. 6. Geological cross section of the Transantarctic Mountain front near the dry valleys (see Figure 5 for location) and a schematic uplift profile relative to a coastal datum [from *Gleadow and Fitzgerald*, 1987]. The uplift (continuous line) is a profile connecting the extrapolated elevations of a preuplift isochron (dots) from apatite fission track analysis which is at sea level at the coast. The total uplift can be found by adding about 4 km of known section above the reference isochron [*Gleadow and Fitzgerald*, 1987]. Small dots are Beacon Sandstone Group; large dots are basement rocks; short lines are Ferrar dolerite sills. The Kukri peneplain separates Beacon Group sediments from basement rocks.

cent to the Transantarctic Mountains (the Ross Sea) is underlain by a thin continental crust resulting from episodic rifting since the late Mesozoic [*Cooper et al.*, 1987, 1991]. Fission track studies indicate a maximum uplift of 5–6 km during the last 60 m.y. (Figure 6 and *Fitzgerald et al.* [1986]).

East Antarctica has had a major ice cap since at least the early Oligocene (36 Ma), although during this time the ice waxed and waned numerous times [*Barrett et al.*, 1989]. The presence of ice on East Antarctica would have inhibited erosion; for example, *Wellman and Tingey* [1981] gave an estimate of the rate of erosion for East Antarctica of about 0.05 km/m.y., which is about an order of magnitude less than erosion rates for other continents from more temperate climates (e.g., southern Africa [*Dingle*, 1982]). The ice-rock contact beneath the East Antarctica ice cap, mapped by high resolution radio echo soundings [*Drewry*, 1976, 1983], is therefore assumed to approximate the uplift profile in the region. This assumption is supported by the similarity in the shape of five widely spaced subice topographic profiles across the Transantarctic Mountains and beneath the ice cap (Figure 7). Furthermore, preserved within the Transantarctic Mountains is a reference level for the slope of the uplift profile. The Kukri peneplain of Devonian age has been subjected to little deformation from the Devonian to the Cenozoic and can, therefore, be used locally as a reference for the horizontal preuplift surface [*Gunn and Warren*, 1962]. On average, the peneplain now dips westward at 2°–3° at a distance of about 40 km from the Ross Sea coast (see *Stern and ten Brink* [1989] for references).

Broken Plate Models

The uplift of the Transantarctic Mountains is modeled here as an upward deflection of a broken elastic plate, with an upward force applied at the boundary zone between the continents of East and West Antarctica (the Ross Embayment) (Figure 4) [*Stern and ten Brink*, 1989]. In the broken elastic plate model, shear forces and bending moments are not transmitted across this boundary, allowing for independent isostatic responses of East and West Antarctica. A broken plate model is used, rather than a continuous elastic plate model, for East and West Antarctica [*Drewry*, 1983], for the following reasons. First, normal faults [*Cooper et al.*, 1987; *Gleadow and Fitzgerald*, 1987], volcanism [*Stump et al.*, 1980], and high heat flow [*Blackman et al.*, 1987] indicate that rifting has occurred recently at this boundary, suggesting that the boundary zone is weak. Second, the dip of the Kukri peneplain in the Transantarctic Mountain sector facing Ross Archipelago was not affected by the volcanic load of Ross Archipelago [*Fitzgerald*, 1991]. Ross Archipelago which includes the volcanoes of Ross Island is located on the extended continental lithosphere of West Antarctica at its boundary with the Transantarctic Mountains.

Figure 7 shows three calculated displacement curves that correspond to equivalent elastic thickness T_e of 90, 115, and 130 km. Figure 7 suggests that the range of flexural rigidities that fits the distance between the Transantarctic Mountains and the Wilkes Basin is limited to an elastic thickness, T_e = 110 ± 20 km. In all three curves, the effective elastic thickness decreases linearly from a distance of about 130 km inland to a value of T_e = 5 km at the plate edge. The decrease in rigidity is necessary to match the 2°–3° dip of the Kukri peneplain [*Stern and ten Brink*, 1989].

Wilkes Basin: A Hinterland Flexural Basin

The Wilkes Basin is a broad and shallow topographic depression behind the Transantarctic Mountains (Figure 5). Little is known about the origin and the age of the subglacial Wilkes Basin or about the sediment thickness in it. Sparse

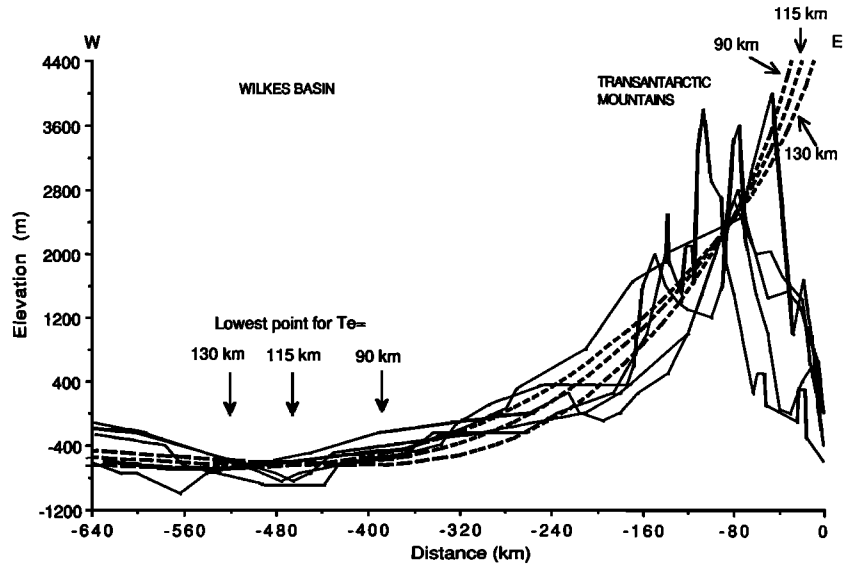

Fig. 7. Stack of five topographic profiles across the Transantarctic Mountains and Wilkes Basin (solid lines, see Figure 5 for location) and modeled curves of deflection of a broken elastic plate with elastic thicknesses of T_e = 90, 115, and 130 km (dashed lines). The absolute elevations of the two southernmost profiles (1 and 2 in Figure 5) have been uniformly shifted down ~500 m to match the other three profiles [see *Stern and ten Brink*, 1989]. Note that the half wavelength of the topography, represented by the location of the lowest elevation, can be fit by a plate with T_e = 115 km but not with T_e = 90 km. The elastic thickness in all three models decreases toward the free edge (at km zero, the coast) in order to match the observed 2–3° dip of the Kukri peneplain 40 km from the coast.

gravity measurements indicate a free-air gravity low of −40 to −50 mGal over the basin (Figure 5).

Our flexural model for the Transantarctic Mountains (Figure 7) implies that Wilkes Basin was formed by a regional isostatic response to uplift at the Transantarctic Mountains. Wilkes Basin is therefore viewed as being analogous, but in the opposite sense, to outer rises adjacent to subduction zones. The broad negative gravity anomaly over the basin supports this interpretation.

Two end-member models for sedimentary basins and their associated free-air gravity effect are illustrated in Figure 8. Figure 8*a* represents a basin few hundred kilometers wide that is locally compensated at the Moho (T_e = 0 km) and that could have formed by uniform extension. This model shows gravity edge effects at the margin of the basin, but, within the basin, the gravity effect approaches zero. Figure 8*b* represents the other end-member where the basin is associated with regional isostasy (large T_e), and the driving force for flexure is located beyond the edge of the basin. The gravity effect Δg of the flexural basin is estimated by the Bouguer slab formula $\Delta g = 2\pi G \cdot \Delta\rho \cdot \Delta z$, where Δz is the flexurally induced displacement, $\Delta\rho$ is the density contrast between the material underlying the elastic plate (the asthenosphere is 3300 kg/m^3) and the infilling material (ice is 900 kg/m^3), and G is the universal gravitational constant. For an elastic plate having a free-edge, the maximum amplitude of the flexural outer bulge, an "outer low" in the present case, is about 7% of the amplitude of the principal uplift [*Turcotte and Schubert*, 1982]. For maximum uplift of ~5000 m of the Transantarctic Mountains, maximum deflection (Δz) of 350 m could be expected in the Wilkes Basin. From the above equation, 350 m of downward deflection would give an observed free-air gravity effect of about −40 mGal, which is close to what is observed (Figure 5). Thus the flexural model is consistent with the gravity observations from Wilkes Basin whereas a local isostasy (Airy) model is not.

Southern Africa: Erosion of the Great Escarpment and Deposition Offshore

The landscape of southern Africa is dominated by the 3000-km-long "Great Escarpment" which is 50–300 km inland from the coast and separates the continental margins of the Indian and Atlantic Oceans from the interior plateau (Figure 9). The axis of highest elevation of southern Africa closely follows the Great Escarpment with elevations ranging between 1500 and 2500 m and in places reaching 3500 m [*Ollier and Marker*, 1985]. An elevated (~1000 m) shallow and broad basin, the Kalahari Basin, is located behind the Great Escarpment of southwestern Africa. The sediments filling the basin, the Kalahari Group, are on average 0–200 m thick (Figure 9).

The continental margin of southwestern Africa can be divided into two zones (Figure 9) [*Austin and Uchupi*, 1982; *Gerrard and Smith*, 1983]: (1) Normal continental crust extends westward to an average distance of 125 km from the coast, and roughly corresponds to the continental shelf with a water depth <500 m. (2) A block-faulted transitional crust is under the continental slope 125–275 km offshore out to an average water depth of 3000 m. Oceanic crust starts only 275 km offshore. The major depocenters along the Atlantic coast are all located within the continental crust or at its boundary with the transitional crust (Figure 9) [*Gerrard and Smith*, 1983]. The largest and deepest depocenter, the Orange Basin, receives its sediments from the Orange-Vaal River, the only significant river breaching the Great Escarpment. A surge in sedimentation rate offshore at ~87 Ma indicates the time at which this breach may have occurred [*Rust and Summerfield*, 1990].

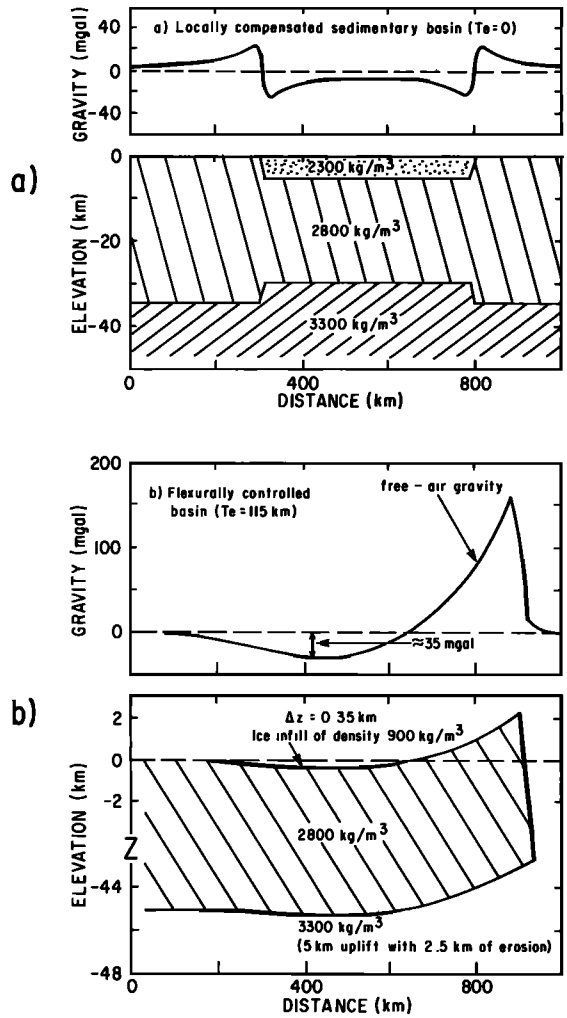

Fig. 8. Simplified isostatic models for locally and regionally compensated sedimentary basins and their associated free-air gravity anomalies. (*a*) Locally compensated wide (400 km) basin formed by crustal thinning due to uniform extension. (*b*) Flexural basin driven by upward loading (uplift) at the edge of the plate. Note that in order to generate comparable amplitude of negative gravity anomaly, the basin in the locally compensated model needs to be much deeper than the flexural basin. This is because the Moho is deflected upward beneath the basin in Figure 8*a* and downward in Figure 8*b*.

A reconstruction of the uplift geometry of southern Africa is difficult because, unlike Antarctica, erosion has been extensive, and a single regional reference horizon similar to the Kukri peneplain is lacking. Exposures of the Etendeka flood basalts between the coast and the Great Escarpment in Namibia (profile D in Figure 9) can locally be used as a reference level (Figure 10, profiles D and E). These flood basalts erupted shortly before seafloor spreading commenced in the South Atlantic and are now flat lying [*Erlank et al.*, 1984]. Where underlain by Mesozoic and Upper Paleozoic sedimentary strata, the lavas follow the latter with apparent conformity [*Erlank et al.*, 1984]. Erosional surfaces can also serve as reference levels, although their chronology and correlation over large areas are more speculative [*Summerfield*, 1985; *Partridge and Maud*, 1987]. Prebreakup and postbreakup erosional surfaces are gently tilted from the Great Escarpment toward both the center of the continent and the coast (Figure 10, profiles A–C [*King*, 1955; *Partridge and Maud*, 1987]). The diminishing elevation of the erosional surfaces of southern Africa toward the coast and the flat-lying basalts and sediments are in marked contrast with the Transantarctic Mountains where the Kukri peneplain is tilted up toward the boundary with West Antarctica.

It has long been recognized [*Suess*, 1904; *King*, 1955; *Martin*, 1976; *Partridge and Maud*, 1987] that the Great Escarpment is an erosional feature which, except locally, is not associated with normal faults [*Miller and Schack*, 1980; *Visser*, 1984]. In contrast, a narrow (<60 km) zone of extensive normal faulting with a vertical throw of 5–7 km is located at the front of the Transantarctic Mountains (Figure 6). Apatite fission track analysis suggests 2.5 km of postrift denudation at the current axis of the Great Escarpment in southwestern Africa and larger amounts of denudation toward the coast [*Brown et al.*, 1991]. This estimate is based on a geotherm of 30°C/km and the assumption that the samples cooled entirely by unroofing. Other geological evidence suggests denudation in excess of 1800 m [*Erlank et al.*, 1984; *Rust and Summerfield*, 1990].

Onshore geomorphic evidence and the relative thicknesses of offshore sedimentary sequences suggest that a major part of the erosion occurred at or immediately after the initiation of seafloor spreading [*Dingle*, 1982; *Gerrard and Smith*, 1983; *Partridge and Maud*, 1987; *Rust and Summerfield*, 1990]. Marine Jurassic sediments in the Cape province indicate that, at least locally, uplift began after the Jurassic [*Sahagian*, 1988]. Analysis of the distance traveled by basalt clasts suggests that by mid-Cretaceous, the Great Escarpment in Natal (SE coast) had receded some 100 km from the coast, and toward the end of the Cretaceous, this distance increased to 120 km, which is not far from its present position [*Partridge and Maud*, 1987]. Apatite fission track ages measured on rocks from the Atlantic coast and the Great Escarpment correlate with the onset of seafloor spreading [*Brown et al.*, 1991]. The single cooling age for all samples along profiles perpendicular to the coast suggests that exhumation lasted 10 m.y. or less [*Brown et al.*, 1991, R. Brown, personal communication, 1989]. About 2/3 of the offshore sediments (corrected for compaction) in the Walvis and Outeniqua basins were deposited during or shortly after the initiation of seafloor spreading (>100 Ma) and most of the remaining 1/3 was deposited before the Cenozoic started (100–65 Ma) [*Dingle*, 1982].

Continuous Plate Models

A ~1200-km-long cross section of southern Africa, extending from the Kalahari Basin to the abyssal plain of the Atlantic Ocean, was modeled using continuous elastic plate models. Modeling the entire cross section together is necessary because some of the loads acting on the plate (erosion and sedimentation) shift their location through time and because the response of a highly rigid plate is felt up to several hundred kilometers away from the loading. Several continuous plate models were compared in which the lateral distribution of elastic thicknesses was varied.

The initial uplift profile of southern Africa was, probably, asymmetric in shape: it rose gradually from ~1000 m in the interior to ~2500 m close to the coast [*Sahagian*, 1988]. For each of the models, the initial uplift profile (e.g., Figure 3) was generated by an upward "load", which decreased

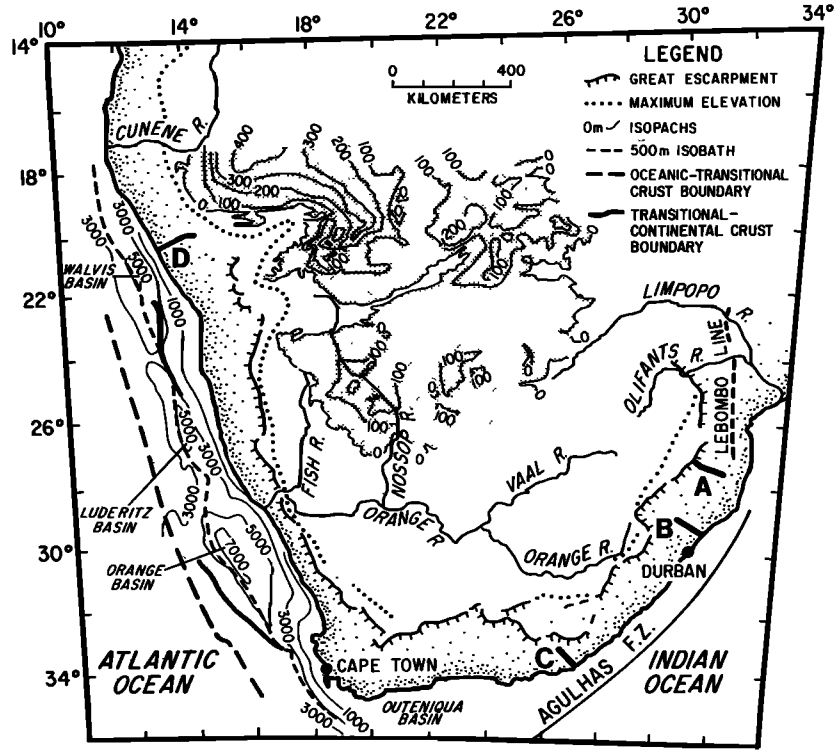

Fig. 9. Map of pertinent morphological, sedimentological, and tectonic features of southern Africa. Location of Great Escarpment after *Ollier and Marker* [1985]. Isopachs of the Kalahari Group compiled from *Botswana Geological Survey Department* [1978] and *Miller and Schalk* [1980]. Isopach map between seafloor and the breakup unconformity (Early Cretaceous) in the Atlantic coast from offshore seismic data after *Gerrard and Smith* [1983]. Heavy lines A, B, C, and D are locations of profiles in Figure 10. Shaded area is geographical extent of Post-Karoo sediments in the Kalahari Basin. Heavy continuous line offshore Atlantic Ocean is seaward extent of continental crust [from *Austin and Uchupi*, 1982]. Heavy dashed line offshore is boundary between oceanic crust and rifted continental or transitional crust [from *Gerrard and Smith*, 1983]. Thin dashed line offshore is the 500-m bathymetric contour.

linearly from the coast to 150 km inland. The upward load was adjusted to reach a maximum of 1500 m near the coast and was superimposed on an 1000-m-high continent-wide plateau [*King*, 1955], which, for lack of any constraints, was assumed to be flat [*Ollier*, 1985]. The initial uplift was assumed to start at the coast. Models where the initial uplift started at the continental edge (125 km from the coast) were tested and found to produce significant erosion and subaerial exposure of the continental shelf, which are not observed.

The thermal subsidence s of the continental margin increased in the models linearly from zero at the coast line to the empirical mid-oceanic ridge subsidence (for $t < 70$ Ma, $s = 2.5 + 0.35 \times t^{1/2}$; for $t > 70$ Ma, $s = 6.4\text{–}3.2 \times \exp(-t/62.8)$ [*Parsons and Sclater*, 1977] at the boundary between the transitional crust and oceanic crust 275 km from shore [*Austin and Uchupi*, 1982].

Three steps of erosion, sedimentation, and rebound 20, 30, and 115 m.y. (present day) after the initial uplift were modeled in which the Great Escarpment retreated by, respectively, 70, 100, and 105 km from the coast (Figure 3). The time steps follow the three major sedimentary sequences identified off the Atlantic coast, which roughly correspond to Early Cretaceous, Late Cretaceous, and the Cenozoic [*Dingle*, 1982; *Gerrard and Smith*, 1983]. The distance of escarpment retreat corresponds to the ratio of sediment thicknesses between these three sequences [*Dingle*, 1982].

Since this paper investigates only the gross features of the transition from continent to ocean, the patterns of erosion and sedimentation were simplified. Instead of tracking realistic angles of sediment repose offshore and slope-dependent erosional rates onshore, the models calculated abrupt terminations of both erosion and sedimentation. These approximations affect local areas such as the shelf edge, but they do not alter the conclusions from the modeling. The effect of sediment compaction is also neglected in the modeling. This is likely to alter the predicted sedimentary thicknesses in the depocenters. The most important effect, however, is the variation in sediment flux to the margin. Much of the African margin is fed by sediments eroded from the front to the Great Escarpment. Where the Orange River breaches the escarpment, the margin is fed by sediments eroded from the hinterland. The difference in sediment flux translates to differences of ~100 km in the width of the continental shelf and 2000–3000 m in the thickness of the depocenters [*Gerrard and Smith*, 1983]. The differences in width and thickness were also verified by the models. Our models were calculated for both sediment flux cases, although only the later case is presented in the figures because the conclusions regarding the isostatic response of the continental margin are similar in both cases.

Model Results

Figure 10 (profile E) compares the predicted final topography from a continuous elastic plate model (after three

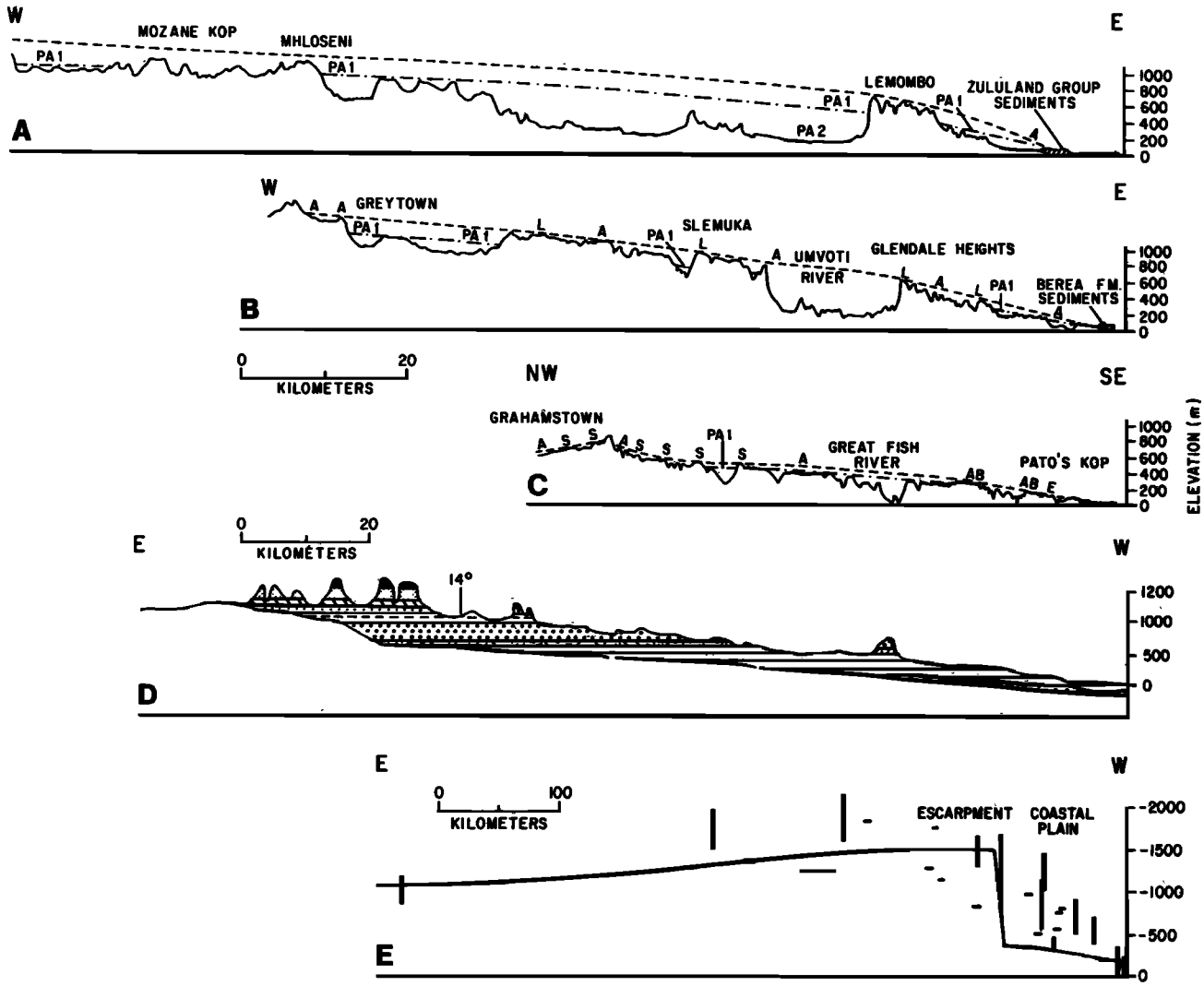

Fig. 10. Profiles A, B, and C are erosional surfaces between the Great Escarpment and the coast [from *Partridge and Maud*, 1987]. See Figure 9 for location. Dashed line is African (A) erosional surface (postbreakup). Dash-dotted line is post-African I (PA1) erosional surface (late Cenozoic). The following notations are AB, African marine platform; E, Eocene marine deposits; L, Laterite; PA2, Post-African II erosional surface; S, silcrete. Profile D is dips of various units (shaded with various patterns) of the Etendeka flood basalts [from *Erlank et al.*, 1984]. Profile E is composite profile perpendicular to the Atlantic margin of southern Africa between latitudes 17° and 24°S showing elevations of the eolian Etjo sandstones (horizontal bars) and Etendeka flood basalts (vertical bars) [after *Martin*, 1976]. The Etendaka basalts erupted at ~120 Ma, and the lowermost flows are interbedded with the Etjo formation of Triassic-Lower Cretaceaous age. The composite profile is compared with the calculated final topography from a continuous elastic plate model with three erosional steps (see text). Model parameters are as in Figure 11, model B.

erosion and rebound cycles) to a composite profile of the elevations of two preuplift markers between latitudes 17°–24°. The markers are the Etendeka flood basalts and the eolian Etjo sandstones. An elastic thickness, T_e = 80 km, is used in the model for the lithosphere of the southern African continent (see discussion in the next section), and a T_e = 10 km is used for the transitional crust under the continental margin [after *Karner and Watts*, 1982]. There is generally good agreement between the composite profile and the predicted elevation from the continuous elastic plate model, except in the coastal plain. The misfit in the coastal plain is due to the simplified erosional scheme of erosion down to sea level seaward of the escarpment.

The following set of models (Figures 11 and 12) investigates the location where the reduction in rigidity occurs, by comparing the predicted final topography, and the predicted total denudation and deposition, to observations. Specifically, the reduction in lithospheric rigidity can occur in one of three zones: A, between the Great Escarpment and the coast (108–0 km onshore); B, between the coast and the seaward edge of the continental crust (0–125 km offshore); and C, within the transitional crust (125–275 km offshore).

Figure 11 compares the predicted final topography to the decreasing elevation of erosional surfaces toward the coast (Figure 10, profiles A–C), the observed dip of the Etendeka basalts at a distance of 100–0 km inland (Figure 10, profile D), and to the gentle dip of the subaqueous continental shelf (Figure 11). Note that only models where the reduction in the elastic thickness occurs at the outer continental shelf (model B) or the continental slope (model C) fit the obser-

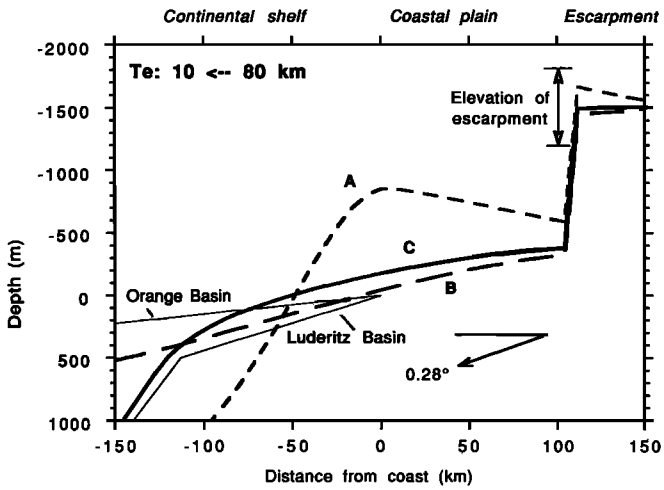

Fig. 11. Final topography of the Great Escarpment, coastal plain, and continental margin from three time-dependent erosional models (A, B, and C). Elastic thickness T_e in all models decreases from T_e = 80 km inland to T_e = 10 km offshore. The models differ in the location at which the change in T_e takes place: Model A, between the escarpment (km 108) and the coast (km 0); model B, between the coast (km 0) and the seaward edge of normal continental crust (−125 km); model C, within the transitional crust (−125 to −275 km). See text and Figure 3 for details of modeling. The models are compared with the following observations: the diminishing elevation of erosional surfaces toward the coast in Figure 10, dip of the Etendeka basalts in Figure 10 (≤0.28° [*Erlank et al.*, 1984]), bathymetry of the continental shelf across the Orange and Luderitz Basins (thin lines [from *Gerrard and Smith*, 1983]), and the elevation range of the Great Escarpment in Namibia (arrows).

vations. Model A, in which the reduction in the rigidity occurs under the coastal plain (T_e = 80 at the Great Escarpment and T_e = 10 km at the coast), predicts, contrary to the observations, an increase in topography toward the coast (which is reminiscent of the predicted topography of the broken plate model, Figure 4) followed by a steep plunge offshore. Increasing the elastic thickness of the oceanic end from 10 to 30 km eliminates the rise in topography toward the coast in model A, but the seaward dip of the continental shelf is still higher than observed. The fits of models B and C are also improved with a T_e = 30 km at the oceanic end.

Figure 12 compares the predicted total thickness of onshore denudation and offshore sediments with the inferred denudation from fission track analysis and to the observed location of depocenters offshore. As in Figure 11, models A, B, and C vary only in the location where the rigidity decreases. All models predict 2.5–3.5 km of denudation at the Great Escarpment (km 108) in agreement with the observations (Figure 12). The predicted thickness of denudation in the coastal plain, 3.25–5 km, in all the models is also larger than the minimum thickness inferred from fission track data. The small predicted thickness of denudation during the last 100–120 m.y. indicates a small amount of erosional rebound in agreement with the absence of many normal faults in the coastal plain. The difference between models A, B, and C appears in the location and amplitude of the depocenters offshore. Model B, in which the elastic thickness under the continental shelf decreases from 80 to 10 km (Figure 12), appears to best fit the location and amplitude of the depocenter, whereas model A predicts substantial erosion (up to 4 km) in the inner shelf (−50 km < x < 0). Comparison between models where the oceanic end has a T_e = 10 km (Figure 12) and T_e = 30 km (not shown) suggests a better fit to the location and amplitude of the Orange Basin depocenter by models with T_e = 10 km.

In conclusion, the modeling suggests that the transition from a high rigidity continental lithosphere to a lower rigidity transitional lithosphere (or to an oceanic lithosphere) occurs close to the continental shelf edge or possibly even farther seaward. The location of this transition affects the geometries of the shelf, the coastal plain and the Great Escarpment and probably also the location of the offshore depocenters. Without detailed modeling of the sedimentary sequences in the outer continental shelf, slope, and rise we cannot unequivocally differentiate between elastic thicknesses of 10 and 30 km in the transitional crust under the continental slope.

Kalahari Basin: The Hinterland Flexural Basin

The interpretation of the Kalahari Basin as a hinterland flexural basin (or an "outer low", Figure 2) implies that the basin subsided simultaneously with the uplift along the west coast of southern Africa following the opening of the South Atlantic Ocean. Late Cretaceous changes in the drainage pattern of the basin from southward flowing to a northward flowing system of fanning channels suggest that the date of the first relative subsidence is indeed between 80 and 100 Ma [*Partridge and Maud*, 1987]. Furthermore, the basal deposits of the Kalahari Group, preserved in diatremes of the southern Kalahari, are of Late Cretaceous age [*Partridge and Maud*, 1987].

Our models suggest that the topography of the interior of southern Africa has evolved through time as parts of the Kalahari Basin, which initially subsided and received sediments, were later uplifted and eroded (see Figure 3 at distances between 400 and 600 km). The vertical movements predicted by the model can be visualized as a wave train of troughs and peaks that progresses inland with time. In our

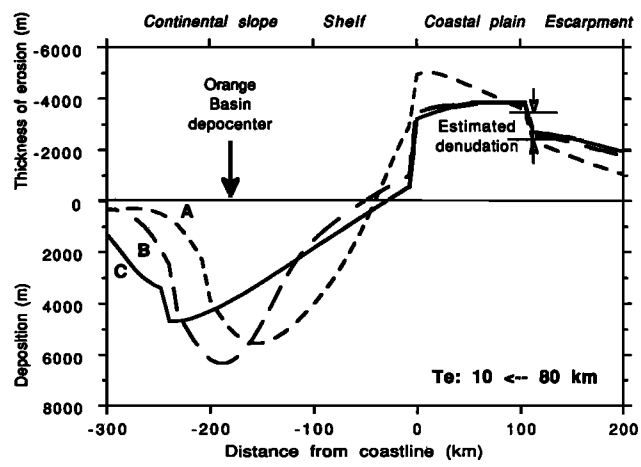

Fig. 12. Distribution of total thickness of erosion and deposition (uncorrected for compaction) from the three time-dependent erosional models (A, B, C) of Figure 11. Elastic thickness T_e in all models decreases from T_e = 80 km inland to T_e = 10 km offshore. The models are compared with the location of the Orange Basin depocenter [from *Gerrard and Smith*, 1983] which derives its sediments from erosion of both the escarpment and the continental interior, and with the estimated range of total denudation at the Great Escarpment [*Brown et al.*, 1991].

models material was removed from elevations above 1000 m inland of the escarpment and deposited into areas of the Kalahari below 1000 m in three steps, and the topography was adjusted isostatically after each step for the changes in load distribution. This simplified pattern of erosion and sedimentation is justified because, in regions of low relief, denudation rate is proportional to elevation [*Stephenson and Lambeck*, 1985] and because the surface of the Kalahari Basin lies at an elevation of ~1000 m.

It is clear from the complex pattern of subsidence and uplift through time that the axis of the outer low will not coincide with the location of maximum thickness of sediments (compare the distance to lowest point in curves for similar T_e in Figures 13*a* and 13*b*). We can, therefore, obtain independent estimates of the elastic thickness of the lithosphere by modeling the distance to the maximum thickness of preserved Kalahari sediments and the distance to the present minimum elevation. Figure 13*a* shows that an elastic thickness of 70–80 km best fits the distance to the thickest Kalahari sediments. Figure 13*b* shows that an elastic thickness of 120 km best fits the distance to the lowest point in the Kalahari Basin, which is 900–1000 km behind the Atlantic coast.

A range of elastic thickness for southern Africa of 80–120 km is consistent with the low geotherm of southern Africa [*Jordan*, 1978; *Jones*, 1988] and with high rigidity determinations of other Gondwana cratons [*Stern and ten Brink*, 1989; *Zuber et al.*, 1989]. The above estimates of elastic thickness are somewhat sensitive to the width of the initial uplift zone, and the elastic thickness can change by 10–20 km depending on the width chosen. The estimates are not, however, sensitive to rigidity variations in the transitional crust of the margin (T_e = 10 km instead of 30 km) because of the large distance to the continental slope.

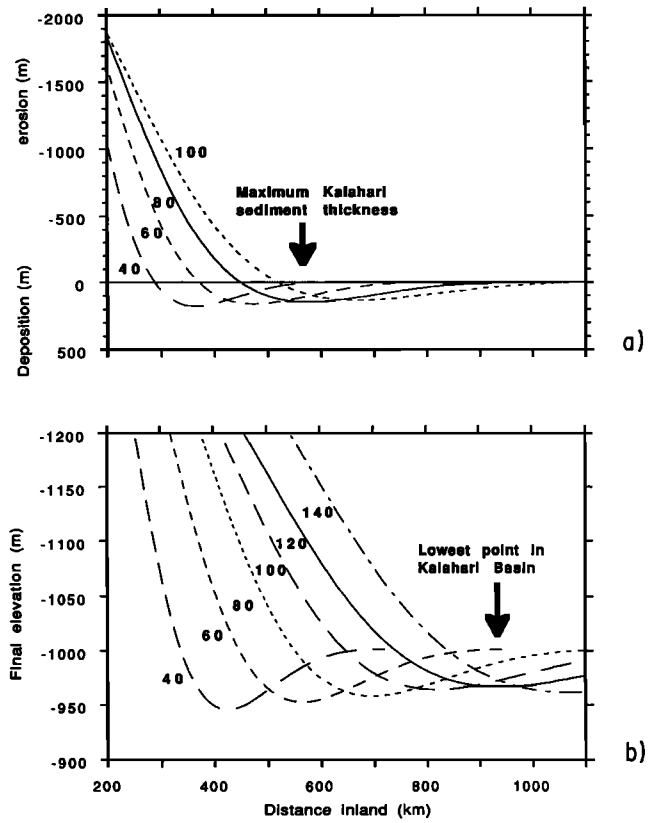

Fig. 13. (*a*) Distribution of the total thickness of erosion (negative) and deposition (positive) in the continental interior (uncorrected for compaction) for models in which the elastic thickness increases from T_e = 30 km under the continental shelf to T_e = 40, 60, 80, or 100 km inland from the coast. Arrow indicates location of observed maximum thickness of Kalahari sediments (~200 m thick) at latitudes 21°–26°S (from Figure 9). (*b*) Final topography for models in which the elastic thickness increases from T_e = 30 km under the shelf to T_e = 40, 60, 80, 100, 120, or 140 km inland from the coast. Arrow indicates location of observed minimum elevation of the Kalahari (900–1000 m above sea level in central Botswana). Note that because erosion and deposition are included in the model, the location of minimum topography (the "outer low") is pushed farther inland than would be predicted from a static flexure model (without erosion and sedimentation) and the outer low does not coincide with the location of maximum sediments.

Discussion

Uplift Forces

This study has highlighted two different types of rift flank uplifts (Figure 1). The contrasting morphology of the two margins can be explained with a model of a broken elastic plate for East Antarctica in which plane stresses are not transmitted between the Transantarctic Mountains and Ross Embayment. For southern Africa, the elastic plate is continuous across the continental margin, and sediment loading offshore subdues the rift flank uplift. Although the Antarctic uplift is young (60–0 Ma) and the African uplift is old (<100 Ma), the differences between Antarctica and southern Africa do not reflect the time since uplift, because most denudation and sedimentation occurred shortly after seafloor spreading began. Hence modeling the African uplift as a continuous plate also applies to the early history of the margin. The difference in the isostatic response between Africa and Antarctica, probably, does not reflect the opening direction of the rift. The Great Escarpment is flanked by both the Atlantic Ocean, which opened perpendicular to the rift flank uplift, and the Indian Ocean, which opened parallel to the rift flank uplift along the Agulhas Fracture Zone (Figure 9), yet the uplift morphology is similar in both cases. The difference in isostatic response between Africa and Antarctica does not reflect the fact that the African rift flanks are adjacent to ocean basins, whereas the Antarctic uplift is adjacent to a stretched continental lithosphere. In fact, the opposite is expected (i.e., a weaker lithosphere next to the African lithosphere) because larger strains and strain rates and higher temperatures are expected during initiation of seafloor spreading than during limited extension (≤ 350–400 km in ~70 Ma in the Ross Sea [*Behrendt and Cooper*, 1991]).

The difference in isostatic response may be caused by differences in the the preexisting structure of the continental lithosphere. The basement under the front of the Transantarctic Mountain may be inherently weak, because it was formed as a collisional fold and thrust belt during Late Precambrian and Early Paleozoic collision and subduction events [e.g., *Davey*, 1987]. The southern Africa continental margins, on the other hand, cut at high angles across Archean to Paleozoic basement blocks [*Eales et al.*, 1984; *Gerrard and Smith*, 1982] and do not seem to follow a potential line of weakness.

Since lithospheric rigidity depends on the thermal structure of the lithosphere [e.g., *Kusznir and Karner*, 1985],

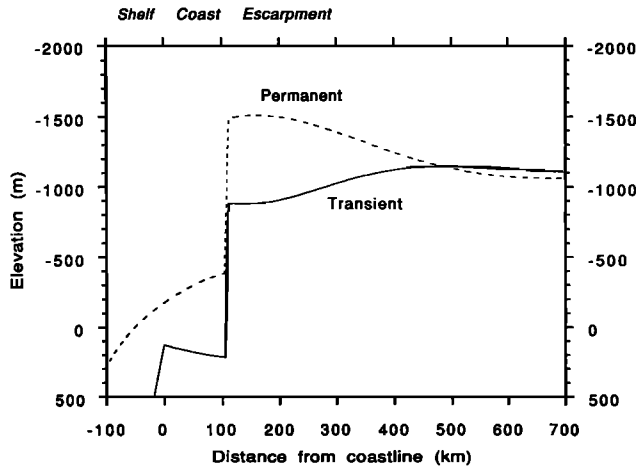

Fig. 14. Comparison between predicted final topography after three erosional cycles for a permanent (dotted line) and a transient (heavy line) initial uplift. Permanent initial uplift model is similar to model B in Figure 11. In the transient uplift model, initial uplift (e.g., due to thermal expansion) decays with square root of time to a negligible value after 115 m.y. (average age of the uplift). The transient uplift model predicts lower elevations than observed in the escarpment and the coastal plain.

lateral variations in the rigidity of the elastic plate are likely to be indicative of lateral thermal variations in the lithosphere. The modeling results for Antarctica indicate a decrease in elastic thickness (T_e = 115 to 5 km) starting about 150 km inland from the boundary between East and West Antarctica that is required to fit the dip of the Kukri peneplain. Brittle and plastic failures due to the high curvature of the uplifted plate edge [e.g., *Bodine et al.*, 1981] are not sufficient to explain all the decrease in elastic thickness. More likely, thermal perturbation from rifting in Ross Embayment extending well into the East Antarctic continental lithosphere is a major cause of the decrease in rigidity toward the edge of the East Antarctic plate (Figure 1). Given enough time (~70 m.y.) excess heat due to horizontal conduction from the Ross Embayment into East Antarctica can indeed explain much of the required uplift force for the Transantarctic Mountains (Appendix A). In contrast, our modeling results for southern Africa indicate that the decrease in elastic thickness there occurs under the continental shelf and slope, not under the coastal plain and the escarpment (Figure 1). The elastic thickness of the lithosphere under the rift-flank uplift (i.e., the present escarpment and the eroded coastal plain) appears to be close to that of the interior, T_e = 80–120 km which implies a thermally thick lithosphere (150–250 km [*McNutt et al.*, 1988]). A further reason that excess heat in the lithosphere cannot explain the uplift of the Great Escarpment is that any thermal uplift should have decayed in the 115 m.y. since seafloor spreading started in the South Atlantic. For example, if the initial uplift in the models discussed earlier is considered thermal and is allowed to decay, the present topography would be markedly different than observed (Figure 14).

For the African margin we suggest that an isostatic mechanism, resulting from lithospheric necking [*Zuber and Parmentier*, 1986; *Braun and Beaumont*, 1989], may explain the extra 1.5 km of required uplift. Some portion of the uplift of the Transantarctic Mountains can also be explained by isostatic rebound across an inclined lithospheric break that is subjected to horizontal tension [*Stern and ten Brink*, 1989; *Bott and Stern*, 1991].

Whereas erosion is an important force that may be responsible for about half of the uplift in both the East Antarctic and the African margins, it cannot by itself cause a rift flank uplift. Denudation of the continental edge after lowering the erosional base level by rift subsidence is insufficient to cause the observed uplift of the Antarctic and African margins, particularly, if the continental lithosphere is highly rigid (Appendix B).

Underplating of the crust may also explain some of the uplift of both margins, although the link between volcanism and permanent uplift is unclear. Surface volcanism in Antarctica is younger than the age of the initiation of uplift [*Stump et al.*, 1980] and extends along a limited portion of the Transantarctic Mountains. Sills and dikes of the Ferrar Dolerites and Kirkpatrick basalt are abundant along much of the Transantarctic Mountains but are much older (Early Jurassic) than the age of uplift [e.g., *Davey*, 1987]. In Namibia, the Etendeka basalts are only slightly older than seafloor initiation and the massive denudation, inferred from fission track analysis, but the geographical spread of the basalts is limited [*Erlank et al.*, 1984]. The Karoo basalts along the southeastern coast are geographically widespread, but their age (191–175 Ma) precedes seafloor spreading by 35–50 m.y. [*Eales et al.*, 1984] and the post-Jurassic uplift in the Cape Province [*Sahagian*, 1988].

In summary, we cannot identify a single force that is responsible for the rift flank uplift of both the Antarctic and the African margins. This leads us to suggest that rift flank uplifts may be due to a combination of forces and that the relative contribution of each of the forces varies between margins.

Hinterland Flexural Basins

Peripheral uplift and wide and shallow hinterland basins may be common in other cratonic areas particularly those associated with the Gondwana supercontinent, for example, the Murry Basin of southeast Australia [*Stephenson and Lambeck*, 1985] and possibly the Nile valley behind the Red Sea hills. We suggest that some vertical movements in the interior of the continent classified as epeirogenic are, in fact, the result of regional isostasy where slow uplift of the rift flank creates a broad subsidence inland. The association is often overlooked because of the large distance between uplift and subsidence. The large distance is a function of the high flexural rigidity of the lithosphere. With a continuous retreat of the escarpment and erosion of interior side of the uplift, the locus of subsidence shifts farther inland with time, and formerly subsided areas are later uplifted (e.g., Figure 3).

The topography, sediment thickness, and free-air gravity anomaly over hinterland basins can be used to estimate the magnitude of the (now partially eroded) uplift. Using an analytical solution to an elastic plate with a constant thickness and no sediments in the "outer low" [*Turcotte and Schubert*, 1982], the maximum amplitude of subsidence of the inland basin should be about 7% of the maximum uplift for a broken elastic plate model and about 4% for a continuous plate model. For example, a maximum cumulative uplift (initial uplift plus erosional rebound) of 5 km is estimated from 200 m of subsidence in the Kalahari Basin.

(The cumulative uplift will be <5 km if sediments fill the 200-m depression.)

The oldest sediments in the basin can be used to document the minimum age for the initiation of uplift if the rift flank uplift and the subsidence of the interior are coupled. For example, the oldest recycled marine fossils found in the terrestrial glacial deposits of the Sirius Formation are of Maastrichtian age (65–74 Ma) [*Webb et al.*, 1984, P.-N. Webb, personal communication, 1989]. *Webb et al.* [1984] believe that these fossils were carried by the ice cap uphill from the Wilkes Basin onto the Transantarctic Mountains where they are now found. We suggest that if these fossils were, indeed, deposited within Wilkes Basin, then the uplift of the Transantarctic Mountains initiated by Maastrichtian time. This suggestion is in accord with the date of the initiation of uplift from fission-track data (~60 Ma (P. Fitzgerald, personal communication, 1989)) and with the initiation of seafloor spreading between the Ross Embayment and the Campbell Plateau (68–73 Ma [*Stock and Molnar*, 1987]).

Conclusions

The principal findings of this paper are as follows:

1. Uplift profiles of the Transantarctic Mountains and the Great Escarpment of southern Africa are consistent with a regional isostatic response to an upward directed force at the rift flank.

2. Morphological differences between the two uplifted rift flanks may reflect variations in the flexural rigidity of the adjacent rifted and extended lithospheres. The topography of the Transantarctic Mountains uplift, which rises toward the mountain front, was best fit by an elastic plate broken at the boundary between East Antarctica and the Ross Embayment, implying negligible rigidity of the extended lithosphere of Ross Embayment close to the mountain front. Geomorphic and geological horizons and the topography of southern Africa, which all warp down toward the continental margin, were best fit by a continuous (although weakened) elastic plate across the continental margin.

3. The difference between the isostatic response of the Transantarctic Mountains and the Great Escarpment may be due to differences in lithospheric strength prior to uplift and is not related to either the amount or the direction of extension or to the time since the extension event took place.

4. From modeled variations in the rigidity across the two margins we infer that the continental lithosphere under the Transantarctic Mountains was heated but the lithosphere under the Great Escarpment was not. This and other geological evidence indicate that a single uplift mechanism has not caused the uplift of both margins.

5. The elastic thickness of the southern African subcontinent is 100 ± 20 km and that of East Antarctica is 110 ± 20 km. These high values appear to be typical of Gondwana cratons.

6. Broad subsidence occurring hundreds of kilometers inland, classified as epeirogenic, may be associated with rift flank uplift along the continental margin. The association is often overlooked because of the large distance between uplift and subsidence, which is a function of both the high flexural rigidity of the lithosphere and the migration of erosion inland. For example, the subsidence of the Kalahari Basin is modeled as a byproduct of the flexural uplift of southwest Africa similar to the subsidence of the Wilkes Basin behind the Transantarctic Mountains. The slow sedimentation rate (200–300 m in 80–100 m.y.) of the wide (>500 km) Kalahari Basin and the wide (>500 km) negative free-air anomaly over the Wilkes Basin are consistent with this explanation. The study of inland basins can, therefore, yield information about the timing and magnitude of the marginal uplift because of the genetic relationship between the two.

Appendix A: Lateral Heat Conduction—A Possible Driving Force for the Uplift of the Transantarctic Mountains

For the Transantarctic Mountains, *Stern and ten Brink* [1989] suggested three principal uplift agents: erosion, an end-load associated with buoyancy forces, and a thermal uplift driven by heat conduction from the warm West Antarctic lithosphere into the cooler lithosphere of East Antarctica. Their combined effect has been used as the driving force for the modeled displacement curves in Figure 7 in the text. Chief among these forces is the possibility of uplift due to density and temperature differences in the upper mantle (Figure A1). The high rigidity of East Antarctica implies a thermal lithosphere 200–250 km thick [*Karner and Watts*, 1983; *McNutt et al.*, 1988]. The Ross Embayment, which is part of the large Cenozoic West Antarctic rift system [*Behrendt and Cooper*, 1991], is probably underlain by a relatively thin thermal lithosphere. In order to obtain a mass balance between the plates of East and West Antarctica (Ross Embayment), which have a large elevation difference as well as a difference in crustal thickness of 15–20 km [*Bentley*, 1983], a density difference of 1–2% between the upper mantles of the two areas is required. The exact density

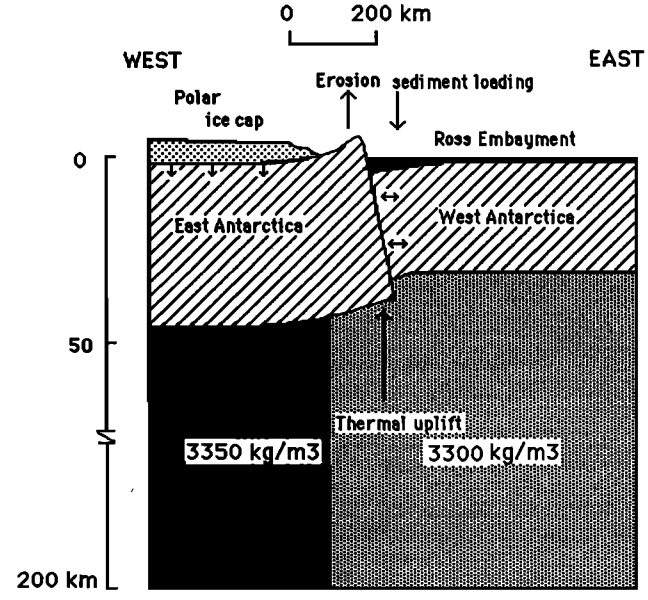

Fig. A1. Illustration of the flexural model and the forces applied on the East-West Antarctic boundary [after *Bott and Stern*, 1991]. Some extension is presumed to exist at the boundary such that the two plates are effectively decoupled along the steep normal fault that separates them. Thermal uplift force is due to heat conduction into East Antarctica. The uplift load due to the weight of the ice cap is insignificant [*Stern and ten Brink*, 1989]. The rigidity of West Antarctica is not well constrained.

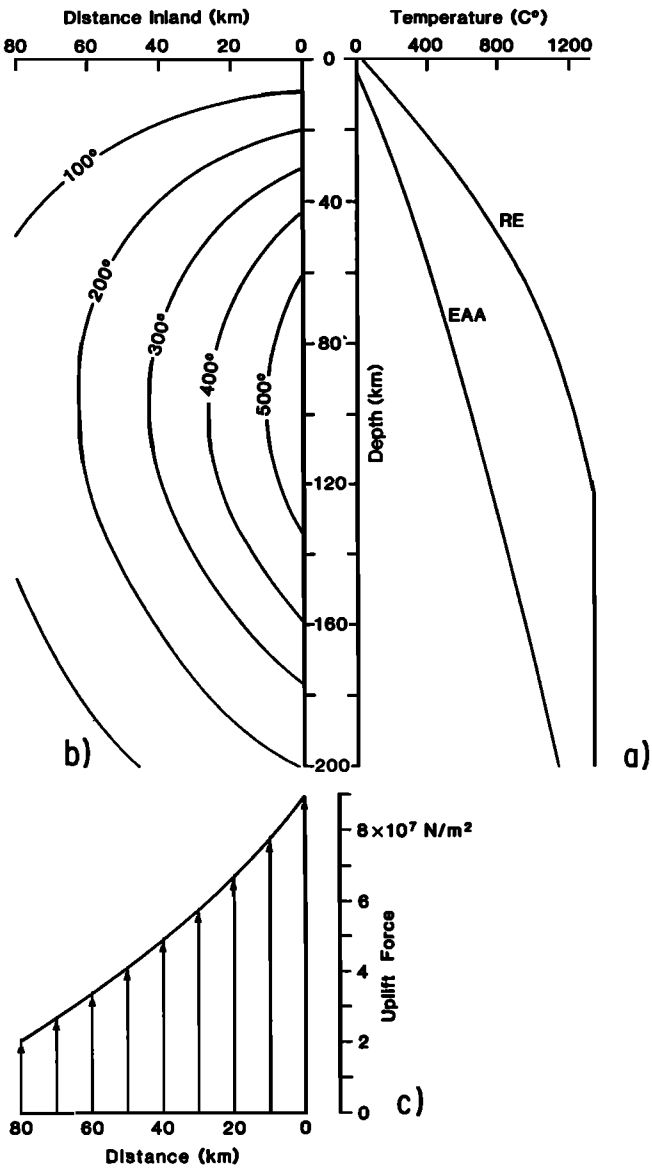

Fig. A2. (*a*) Estimated temperature gradients (geotherms) for the East Antarctica craton (labeled EAA) and for the Ross Embayment (labeled RE). The geotherm for East Antarctica is calculated using a 250-km-thick [*Karner and Watts*, 1983; *McNutt et al.*, 1988] cooling plate model with a thermal age of 530 Ma, which corresponds to the age of the Ross orogeny, the latest widespread orogeny in East Antarctica [*Davey*, 1987]. Bedrock temperature below the ice is −30°C [*McGinnis*, 1979] and radiogenic heat generation is exponentially distributed with depth within the crust. The calculated geotherm for East Antarctica is in agreement with geotherms in other stable continental terrains estimated from geothermometry data [*Jordan*, 1978; *Jones*, 1988] and surface heat flow [*Pollack and Chapman*, 1977]. The depth to 600°C in the calculated geotherm for East Antarctica also matches the thickness of the elastic plate [*Kusznir and Karner*, 1985]. The geotherm for Ross Embayment is calculated using a 125-km-thick cooling plate with an effective thermal age of 70 m.y. and is in accord with the measured heat flow values at the surface [*Blackman et al.*, 1987]. (*b*) Contours of calculated excess temperature in the East Antarctic lithosphere 70 Ma after juxtaposition with the hotter lithosphere of Ross Embayment. The Ross Embayment geotherm is assumed to have remained constant during the last 70 m.y. because of episodic extension in Ross Embayment throughout this period [*Cooper et al.*, 1987, 1991]. (*c*) The integrated buoyant force as a function of distance from the boundary with the Ross Embayment due to the excess temperatures shown in Figure A2*b* and assuming a coefficient of thermal expansion of 3.4×10^{-5} K^{-1}.

difference depends on the choice of the depth of compensation. If the higher temperatures (i.e., lesser density) of the upper mantle of Ross Embayment propagate by conduction with time under part of the Transantarctic Mountains, then the excess heat will provide a buoyant force for the uplift of the Transantarctic Mountains (Figure A2*a*).

We can examine this idea more quantitatively by looking at the effects of heat conduction between the two lithospheres. Estimated steady state temperature gradients throughout the lithosphere (geotherms) for East and West Antarctica are shown in Figure A2*a*. The average temperature difference in the upper mantle between these two geotherms is about 450°C. If the coefficient of thermal expansion is 3.4×10^{-5} K^{-1}, this temperature difference corresponds to a density difference of 1.5%. The calculated density difference matches the 1–2% estimate deduced from mass balance between East Antarctica and the Ross Embayment.

The juxtaposition of two very different geotherms for 70 Ma (assuming that the Ross Embayment geotherm was maintained constant throughout that period) would have led to a lateral heat conduction from the Ross Embayment into the upper mantle under the Transantarctic Mountains. The present anomalous temperatures under East Antarctica following this juxtaposition are shown as a function of distance from its boundary with the Ross Embayment (Figure A2*b*). The anomalous lateral temperature distribution under the Transantarctic Mountains is translated into density variations, which act as a distributed upward force (Figure A2*c*) in the flexural modeling of the Transantarctic Mountains. The combined lateral density variation and the erosion following the uplift can account for almost 90% of the driving uplift force required to produce the displacement curves of Figure 7 in the text. The uplift force in Figure A2*c* represents a conservative estimate because geothermometric measurements from McMurdo Sound [*Berg et al.*, 1989] suggest much higher crustal temperatures than estimated for the Ross Embayment (Figure A2*a*) and because a geotherm of 70-m.y.-old oceanic lithosphere is used for the Ross Embayment.

Appendix B: Relationship of Erosion to Isostatic Rebound in a Rigid Lithosphere

King [1955], *Ollier* [1985] and others suggested that the entire southern African landscape was about 1000 m high when the breakup of Gondwana lowered the base level for erosion from 1000 m to sea level at the continental margins (insert in Figure B1). The present topography of southern Africa is, according to King and Ollier, due entirely to the subsequent erosional rebound. We next demonstrate that erosion by itself cannot produce the inferred thickness of denudation (2500–3500 m, from fission track analysis and geological considerations) at the Great Escarpment and that an additional driving force under the margin is necessary.

We look at the erosion of the rectangular edge of a plateau with height Z and width w to sea level (insert in Figure B1). After the rectangle is eroded to sea level, the substratum rebounds isostatically to some height above sea level. The section above sea level is eroded again to sea level, after which another rebound occurs, and so on. If local Airy isostasy is assumed, then, for a given reduction in plateau elevation Z the total thickness of erosion E after many iterations is

$$E = Z + Zr + Zr^2 + Zr^3 + \cdots = Z/(1 - r) \quad \text{(B1)}$$

where the density ratio r is

$$r = \rho_s/\rho_m \quad \text{(B2)}$$

and ρ_s and ρ_m are the densities of the eroded surface material and the upper mantle, respectively.

We name the ratio E/Z, the amplification ratio for erosion. If ρ_s = 2670 kg/m^3 and ρ_m = 3300 kg/m^3, then the amplification ratio is 5.2; that is, the total thickness of erosion is 5.2 times larger than the reduction in elevation.

If, however, isostatic rebound is regional (nonzero rigidity), then for a given reduction in elevation, the amplification ratio is much smaller and is spatially variable. Although a generalized analytic relationship similar to (1) cannot be derived for an eroded rectangle (insert in Figure B1), we can estimate the upper bound of the amplification ratio. The maximum isostatic rebound y of a continuous elastic plate due to an erosion of a rectangle of material occurs at the center of the rectangle, $x = w/2$, and is given by [*Hetenyi*, 1946]

$$y(w/2) = Z\rho_s/\rho_m[1 - e^{-w/2\alpha} \cos (w/2\alpha)] \quad \text{(B3)}$$

where the flexural parameter α is proportional to the rigidity of the plate or its elastic thickness.

Equation (B1) can be used to calculate the upper limit for the amplification ratio under the condition of regional isostasy if we assume that the entire rectangular area rebounds and erodes to a constant level, which is that of the center. For regional isostasy, the modified density ratio r is then

$$r < \rho_s/\rho_m[1 - e^{-w/2\alpha} \cos (w/2\alpha)] \quad \text{(B4)}$$

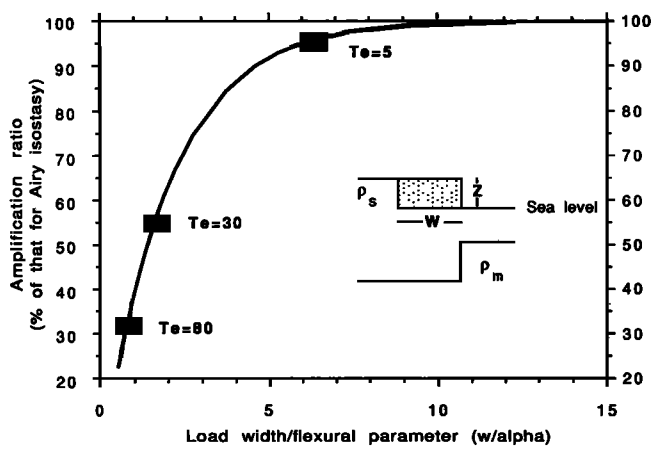

Fig. B1. Heavy curve is amplification ratio for regional isostasy (normalized by the amplification ratio for local Airy isostasy) as a function of nondimensional flexural parameter (width of eroded block, w, divided by flexural parameter, α). An amplification ratio is the ratio between the thickness of erosion in the limit and the decrease in elevation due to erosion. For Airy isostasy, this ratio is calculated analytically, but for regional isostasy, only an upper bound can be calculated. The flexural parameter is proportional to the elastic thickness T_e in the power of 3/4. Solid rectangles are amplification ratio for T_e = 5, 30, and 80 km and an eroded block with a width of 105 km, which is a typical distance between the Atlantic coast and the Great Escarpment of southern Africa. Inset is a sketch of the model used to calculate the amplification ratio: Erosion of a rectangle of continental material (dotted) of height Z and width w following the creation of ocean basin which lowered the base level.

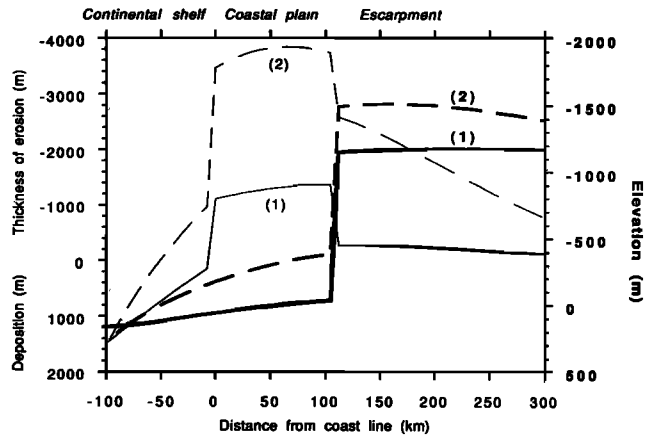

Fig. B2. Comparison of final topography (heavy lines) and total thickness of erosion (thin lines) between two models that differ in their uplift geometries: (1) Initial flat plateau of 1000 m extending from the interior to the coast; (2) Gradual increase in elevation from 1000 m in the interior to 2500 m near the coast (similar to initial uplift in Figure 4 in text).

The inequality sign is used since the actual flexural rebound deviates from the simplifying assumption of a rebound to a constant level and is smaller toward the edges of the block. The modified ratio r depends on the width of the rectangle and the flexural rigidity (via the flexural parameter). When $\alpha \to \infty$ or $w \to 0$; $r \to 0$ and $E = Z$. When $\alpha \to 0$ or $w \to \infty$; $r \to \rho_s/\rho_m$, the local Airy case.

Note that the modified density ratio (equation (B4)) is always smaller than the simple density ratio (equation (B2)); hence the amplification ratio will always be smaller for regional isostasy than for local isostasy. Moreover, the amplification ratio decreases as the rigidity (elastic thickness) increases. Figure B1 shows the amplification ratio as a percentage of the amplification ratio for a purely Airy isostasy. For a load width of w = 105 km (the distance between the coast and the Great Escarpment) and an elastic thickness of T_e = 30 km, the amplification ratio is 55% that of an Airy compensation. For a T_e = 80 km, a value advocated for the Great Escarpment, the amplification ratio is only 32%. Hence, if the average change in elevation (from the initial 1000-m-high uniform elevation of southern Africa) between the coast and the Great Escarpment, ΔZ = 500 m, the total thickness of erosion E between the coast and the escarpment is <1430 m (for T_e = 30 km) or <830 m (for T_e = 80 km). This is much less than the estimated minimum thickness of erosion, E > 2500–3500 m between the coast and the Great Escarpment suggesting, therefore, the presence of an additional uplift force close to the continental edge.

Expression (B4) represents an upper bound for the modified density ratio r not only because r is smaller approaching the edges of the block but also because the eroded material is likely to be deposited near by and constitute a downward load which further inhibits erosional rebound. These factors have been taken into consideration in the numerical model, shown in Figure B2. This model, which in all but the magnitude of initial topography is similar to the other models in this study, cannot produce the 2500–3500 m of observed denudation or the current elevation (~1500 m) of the escarpment.

Acknowledgments. We thank P. Barrett, R. Brown, A. Cooper, P. Fitzgerald, G. Quinlan, E. Robinson, N. Sleep, G. Thompson, and R. Walcott for reviewing earlier versions of this manuscript. Dork Sahagian and Roderick Brown introduced us to the African literature, and Roderick Brown and Paul Fitzgerald kindly provided preprints of their work. Reviews by Sarah Kruse, Tom Brocher, Kim Klitgord, Alan Cooper, and an anonymous reviewer helped improve the manuscript. This work was supported by National Science Foundation grants DPP-8813162 and DPP-8917634.

REFERENCES

Austin, J. A., and E. Uchupi, Continental-oceanic crustal transition off southwest Africa, *AAPG Bull.*, *66*, 1328–1347, 1982.

Barrett, P. J., M. J. Hambrey, D. M. Harwood, A. R. Pyne, and P.-N. Webb, Synthesis, in Antarctic Cenozoic history From the CIROS-1 Drill Hole, McMurdo Sound, edited by P. J. Barrett, *DSIR Bull. N. Z.*, 241–251, *245*, 1989.

Behrendt, J. C., and A. K. Cooper, Evidence of rapid Cenozoic uplift of the shoulder escarpment of the Cenozoic West Antarctic rift system and a speculation on possible climate forcing, *Geology*, *19*, 315–319, 1991.

Bentley, C. R., Crustal structure of Antarctica from geophysical evidence—A review, in *Antarctic Earth Science*, edited by R. L. Oliver, P. R. James, and J. B. Jago, pp. 491–497, Australian Academy of Sciences, Canberra, Australia, 1983.

Berg, J. H., R. J. Moscati, and D. L. Herz, A petrologic geotherm from a continental rift in Antarctica, *Earth Planet. Sci. Lett.*, *93*, 98–108, 1989.

Blackman, D. K., R. P. Von Herzen, and L. A. Lawver, Heat flow and tectonics in the western Ross Sea, in *The Antarctic Continental Margin, Geology and Geophysics of the Western Ross Sea, Earth Sci. Ser.*, vol. 5B, edited by A. K. Cooper and F. J. Davey, pp. 179–190, Circum-Pacific Council for Energy and Mineral Resources, Houston, Tex., 1987.

Bodine, J. H., M. S. Steckler, and A. B. Watts, Observations of flexure and the rheology of the oceanic lithosphere, *J. Geophys. Res.*, *86*, 3695–3707, 1981.

Botswana Geological Survey Department, Reconnaissance aeromagnetic survey, synoptic interpretation map, scale 1:1000000, sheets 1, 2, Gaborone, 1978.

Bott, M. H. P., and T. A. Stern, Finite element analysis of Transantarctic Mountains uplift and coeval subsidence in the Ross Embayment, *Tectonophysics*, in press, 1991.

Braun, J., and C. Beaumont, A physical explanation of the relation between flank uplifts and the breakup unconformity at rifted continental margins, *Geology*, *17*, 760–764, 1989.

Brown, R. W., Backstacking apatite fission-track "stratigraphy": A method for resolving the erosional and isostatic rebound components of tectonic uplift histories, *Geology*, *19*, 74–77, 1991.

Brown, R. W., D. J. Rust, M. A. Summerfield, A. J. W. Gleadow, and M. C. J. De Wit, An Early Cretaceous phase of accelerated erosion on the south western margin of Africa: Evidence from fission track analysis and the off-shore sedimentary record, *Nucl. Tracks, Radiat. Meas.*, *17*, 339–350, 1991.

Buck, W. R., Small-scale convection induced by passive rifting, the cause for uplift of rift shoulders, *Earth Planet. Sci. Lett.*, *77*, 362–372, 1986.

Cooper, A. K., F. J. Davey, and J. C. Behrendt, Seismic stratigraphy and structure of the Victorialand basin, western Ross Sea, Antarctica, in *The Antarctic Continental Margin, Geology and Geophysics of the Western Ross Sea, Earth Sci. Ser.*, vol. 5B, edited by A. K. Cooper and F. J. Davey, pp. 27–76, Circum-Pacific Council for Energy and Mineral Resources, Houston, Tex., 1987.

Cooper, A. K., F. J. Davey, and K. Hinz, Crustal extension and origin of sedimentary basins beneath the Ross Sea and the Ross Ice Shelf, Antarctica, in *Geological Evolution of Antarctica*, edited by M. R. A. Thompson et al., pp. 285–291, Cambridge University Press, New York, 1991.

Cox, K. G., A model for flood basalt volcanism, *J. Petrol.*, *21*, 629–630, 1980.

Dalziel, I. W. D., and D. H. Elliot, West Antarctica: problem child of Gondwanaland, *Tectonics*, *1*, 3–20, 1982.

Davey, F. J., Geophysical studies in the Ross Sea region, *J. R. Soc. N. Z.*, *11*, 465–479, 1981.

Davey, F. J., Geology and structure of the Ross Sea region, in *The Antarctic Continental Margin, Geology and Geophysics of the Western Ross Sea, Earth Sci. Ser.*, vol. 5B, edited by A. K. Cooper and F. J. Davey, pp. 1–16, Circum-Pacific Council for Energy and Mineral Resources, Houston, Tex., 1987.

Dingle, R. V., Continental margin subsidence: a comparison between the east and west coasts of Africa, in *Dynamics of Passive Margins, Geodyn. Ser.*, vol. 6, edited by R. A. Scrutton, pp. 59–71, AGU, Washington, D. C., 1982.

Drewry, D. J., Sedimentary basins of the East Antarctic craton from geophysical evidence, *Tectonophysics*, *36*, 301–314, 1976.

Drewry D. J. (Ed.), *Glaciological and Geophysical Folio*, Scott Polar Research Institute, Cambridge, England, 1983.

Eales, H. V., J. S. Marsh, and K. G. Cox, The Karoo igneous province: An introduction, in Petrogenesis of the Volcanic Rocks of the Karoo Province, edited by A. J. Erlank, *Spec. Publ. Geol. Soc. S. Afr.*, *13*, 1–26, 1984.

Erlank, A. J., J. S. Marsh, A. R. Duncan, R. McG. Miller, C. J. Hawkesworth, P. J. Betton, and D. C. Rex, Geochemistry and petrogenesis of the Etendeka volcanic rocks from SWA/Namibia, in Petrogenesis of the Volcanic Rocks of the Karoo Province, edited by A. J. Erlank, *Spec. Publ. Geol. Soc. S. Afr.*, *13*, 196–245, 1984.

Fitzgerald, P. G., The Transantarctic Mountains of southern Victoria Land: The application of fission track analysis to a rift shoulder uplift, *Tectonics*, in press, 1991.

Fitzgerald, P. G., M. Sandiford, P. J. Barrett, and A. J. W. Gleadow, Asymmetric extension associated with uplift and subsidence in the Transantarctic Mountains and the Ross Embayment, *Earth Planet. Sci. Lett.*, *81*, 67–78, 1986.

Gerrard, I., and G. C. Smith, Post-Paleozoic succession and structure of the southwestern African continental margin, in Studies in Continental Margin Geology, edited by J. S. Watkins and C. L. Drake, *AAPG Mem.*, *34*, 49–74, 1983.

Gleadow, A. J. W., and P. G. Fitzgerald, Uplift history and structure of the Transantarctic Mountains: New evidence from fission track dating of basement apatite in the Dry Valleys area, southern Victoria Land, *Earth Planet. Sci. Lett.*, *82*, 1–14, 1987.

Groushinsky, N. P., and N. B. Sazhina, Gravity map of Antarctica, scale 1:5,000,000, Sternberg Astron. Inst. and NII Zarubezhgeology, Moscow, 1978.

Gunn, B. M., and G. Warren, Geology of Victoria Land between the Mawson and Mulock Glaciers, Antarctica, *N. Z. Geol. Surv. Bull.*, *71*, 151 pp., 1962.

Heiskanen, W. A., and F. A. Vening-Meinesz, *The Earth and Its Gravity Field*, 470 pp., McGraw-Hill, New York, 1958.

Hetenyi, M., *Beams on an Elastic Foundation*, 255 pp., University of Michigan Press, Ann Arbor, 1946.

Jones, M. Q. W., Heat flow in the Witwatersrand basin and environs and its significance for the South African shield geotherm and lithosphere thickness, *J. Geophys. Res.*, *93*, 3243–3260, 1988.

Jordan, T. H., Composition and development of the continental tectosphere, *Nature*, *274*, 544–548, 1978.

Karner, G. D., and A. B. Watts, On isostasy of Atlantic-type continental margins, *J. Geophys. Res.*, *87*, 2923–2948, 1982.

Karner, G. D., and A. B. Watts, Gravity anomalies and flexure of the lithosphere at mountain ranges, *J. Geophys. Res.*, *88*, 10,449–10,477, 1983.

Kienle, J., T. F., Redfield, and F. Heimberg, Gravity investigation in the Mt. Melbourne quadrangle, Northern Victoria Land: Constraints on crustal structure of the Transantarctic Mountains (abstract), *Eos Trans. AGU*, *70*, 1362, 1989.

King, L. C., Pediplanation and isostasy: An example from South Africa, *Q. J. Geol. Soc. London*, *111*, 353–359, 1955.

Kusznir, N., and G. D. Karner, Dependence of the flexural rigidity of the continental lithosphere on rheology and temperature, *Nature*, *316*, 138–142, 1985.

Martin, H., A geodynamic model for the evolution of the continental margin of southwestern Africa, *An. Acad. Bras. Cienc.*, *48*, 169–177, 1976.

McGinnis, L. D., Cooling mechanisms and effects on mantle convection beneath Antarctica, *J. Hydrol.*, *43*, 265–286, 1979.

McGinnis, L. D., R. H. Bowen, J. M. Erikson, B. J. Allred, and J. L. Kreaner, East-West Antarctic boundary in McMurdo Sound, *Tectonophysics*, *114*, 341–356, 1985.

McNutt, M. K., M. Diament, and M. G. Kogan, Variations of

elastic plate thickness at continental thrust belts, *J. Geophys. Res.*, *93*, 8825–8838, 1988.
Miller, R. M., and K. E. L. Schalk (Compilers), South West Africa/Namibia geological map, scale 1:1000000, sheets 1-4, Geol. Surv. of the Repub. of S. Afr. and South West Africa/Namibia, Pretoria, 1980.
Ollier, C. D., Morphotectonics of passive continental margins: Introduction, *Z. Geomorphol. Suppl.*, *54*, 1–9, 1985.
Ollier, C. D., and M. E. Marker, The Great Escarpment of southern Africa, *Z. Geomorphol. Suppl.*, *54*, 37–56, 1985.
Parsons, B., and J. G. Sclater, An analysis of the variation of ocean floor bathymetry and heat flow with age, *J. Geophys. Res.*, *82*, 803–827, 1977.
Partridge, T. C., and R. R. Maud, Geomorphic evolution of southern Africa since the Mesozoic, *S. Afr. J. Geol.*, *90*, 179–208, 1987.
Pollack, H. N., and D. S. Chapman, On the regional variation of heat flow, geotherms, and lithospheric thickness, *Tectonophysics*, *38*, 279–296, 1977.
Rust, D. J., and M. A. Summerfield, Isopach and borehole data as indicators of rifted margin evolution in southwestern Africa, *Mar. Pet. Geol.*, *7*, 277–287, 1990.
Sahagian, D., Epeirogenic motions of Africa as inferred from Cretaceous shoreline deposits, *Tectonics*, *7*, 125–138, 1988.
Smith, A. G., and D. J. Drewry, Delayed phase change due to hot asthenosphere causes Transantarctic uplift?, *Nature*, *309*, 536–538, 1984.
Steckler, M. S., Uplift and extension at the Gulf of Suez: Indications of induced mantle convection, *Nature*, *317*, 135–139, 1985.
Stephenson, R., and K. Lambeck, Erosion-isostatic rebound models for uplift: an application to south-eastern Australia, *Geophys. J. R. Astron. Soc.*, *82*, 31–55, 1985.
Stern, T. A., and U. S. ten Brink, Flexural uplift of the Transantarctic Mountains, *J. Geophys. Res.*, *94*, 10,315–10,330, 1989.
Stock, J., and P. Molnar, Revised history of early Tertiary plate motion in the south-west Pacific, *Nature*, *325*, 495–499, 1987.
Stump, E., M. F. Sheridan, S. G. Borg, and J. F. Sutter, Early Miocene subglacial basalts, the East Antarctic ice sheet and uplift of the Transantarctic Mountains, *Science*, *207*, 757–759, 1980.
Suess, E., *The Face of the Earth*, vol. 1, 604 pp., Clarendon Press, Oxford, 1904.
Summerfield, M. A., Plate tectonics and landscape development on the African continent, in *Tectonic Geomorphology*, edited by M. Morisawa and J. J. Hack, pp. 27–51, Allen and Unwin, Boston, Mass., 1985.
Turcotte, D. L., and G. Schubert, *Applications of Continuum Physics to Geological Problems*, 450 pp., John Wiley, New York, 1982.
Visser, D. J. L. (Compiler), Geological map of the republics of South Africa, Transkei, Bophuthatswana, Venda, and Ciskei and the kingdoms of Lesotho and Swaziland, scale 1:1,000,000, 4 sheets, S. Afr. Dep. of Miner. and Energy Affairs, Pretoria, 1984.
Webb, P. N., D. M. Harwood, B. C. McKelvey, J. H. Mercer, and L. D. Stott, Cenozoic marine sedimentation and ice-volume on the East-Antarctic craton, *Geology*, *12*, 287–291, 1984.
Weissel, J., and G. D. Karner, Flexural uplift of rift flanks due to mechanical unloading of the lithosphere during extension, *J. Geophys. Res.*, *94*, 13,919–13,950, 1989.
Wellman, P., and R. J. Tingey, Glaciation, erosion, and uplift over part of East Antarctica, *Nature*, *291*, 142–144, 1981.
Zuber, M. T., and E. M. Parmentier, Lithospheric necking: A dynamic model for rift morphology, *Earth Planet. Sci. Lett.*, *77*, 373–383, 1986.
Zuber, M. T., T. D. Bechtel, and D. W. Forsyth, Effective elastic thicknesses of the lithosphere and mechanisms of isostatic compensation in Australia, *J. Geophys. Res.*, *94*, 9353–9367, 1989.

T. Stern, DSIR-Geology and Geophysics Division, P. O. Box 1320, Wellington, New Zealand.
U. ten Brink, U.S. Geological Survey, Quissett Campus, Woods Hole, MA 02543.

(Received March 14, 1990;
revised August 15, 1991;
accepted August 29, 1991.)